Geophysical Journal International

Geophys. J. Int. (2021) **224,** 1211–1224
Advance Access publication 2020 October 16
GJI Seismology

doi: 10.1093/gji/ggaa499

New measurements of long-period radial modes using large earthquakes

S. Talavera-Soza and A. Deuss

Department of Earth Sciences, Utrecht University, Princetonlaan 8A, 3584CB Utrecht, The Netherlands. E-mail: s.a.talaverasoza@uu.nl

Accepted 2020 October 14. Received 2020 September 23; in original form 2020 February 16

SUMMARY

Radial modes, ${}_nS_0$, are long-period oscillations that describe the radial expansion and contraction of the whole Earth. They are characterized only by their centre frequency and quality factor Q, and provide crucial information about the 1-D structure of the Earth. Radial modes were last measured more than a decade ago using only one or two earthquakes. Here, we measure radial modes using 16 of the strongest and deepest earthquakes of the last two decades. By introducing more earthquake data into our measurements, we improve our knowledge of 1-D attenuation, as we remove potential earthquake bias from our results. For mode ${}_0S_0$, which is dominated by compressional energy, we measure a Q value of 5982, much higher than previously measured, and requiring less bulk attenuation in the Earth than previously thought. We also show that radial modes cross-couple (resonate) strongly to their nearest spheroidal mode due to ellipticity and inner core cylindrical anisotropy. Cross-coupling improves the fit between data and synthetics, and gives better estimates of the centre frequency and attenuation value of the radial modes. Including cross-coupling in our measurements results in a systematic shift of the centre frequencies of radial modes towards the Preliminary Reference Earth Model. This shift in centre frequencies, has implications for the strength of the radial anisotropy present in the uppermost inner core, with our cross-coupling results agreeing with lower values of anisotropy than the ones inferred from just measuring the modes in self-coupling (isolation). Furthermore, cross-coupling between radial modes and angular-order two modes provides constraints on cylindrical inner core anisotropy, that will help us improve our knowledge of the 3-D structure of the inner core.

Key words: Core; Seismic attenuation; Surface waves and free oscillations; Theoretical seismology.

1 INTRODUCTION

Radial modes are long period oscillations involving the radial expansion and contraction of the whole Earth. They provide crucial information about the 1-D structure of the Earth, because they are only described by their centre frequency f_c and quality factor Q. Radial modes are characterized by their low attenuation and corresponding high Q values (Dziewonski & Gilbert 1972) and are visible for many days and sometimes even weeks in the spectra of the largest earthquakes. They are dominated by compressional energy, which is dissipated much more slowly than shear energy. Thus, radial modes are especially important in modelling and constraining 1-D bulk attenuation.

Radial mode Q measurements are often combined with other normal modes to make 1-D models of attenuation (Sailor & Dziewonski 1978; Widmer *et al.* 1991; Durek & Ekström 1995, 1996), as well as with surface and body waves (Anderson & Hart 1978; Dziewonski & Anderson 1981; Durek & Ekström 1995; Masters & Widmer 1995; Durek & Ekström 1996; Romanowicz & Durek 2000; Resovsky *et al.* 2005). These models mainly constrain shear wave attenuation, but in order to fit the radial modes the models also require a region with bulk attenuation Q_κ somewhere in the Earth. Some studies place the region of finite Q_κ in the upper mantle (Sailor & Dziewonski 1978) or the lithosphere (Durek & Ekström 1995), while other studies prefer the inner core (Anderson & Hart 1978; Dziewonski & Anderson 1981) or even the outer core or lower mantle (Resovsky *et al.* 2005). These studies show little agreement on the location of a finite Q_κ in the Earth and new constraints on radial mode Q values are essential to answer this question.

In the past, only one earthquake, and sometimes even only one station, was used to measure radial modes. All studies published before 1995, used one of the same four large events, and performed stacking and weighting due to the lack of available data (Dratler *et al.* 1971; Dziewonski & Gilbert 1972, 1973; Sailor & Dziewonski 1978; Buland *et al.* 1979; Riedesel *et al.* 1980; Masters & Gilbert 1983; Park 1990; Widmer *et al.* 1991; Durek & Ekström 1995;

Okal 1996). He & Tromp (1996) were the first to measure radial modes with more than one event, using the great 1994 Bolivia and Kuril Islands earthquakes. More recently, Okal & Stein (2009) and Roult *et al.* (2010) measured the longest period radial modes using the great Sumatra earthquake of 2004. Here, our aim is to improve normal mode measurements by significantly increasing the number of events and include all events of the last 25 yr that are large enough to show radial mode observations.

Moreover, we are improving some of the theoretical assumptions that have been made in the past when measuring radial modes. Previous studies measured radial modes using the self-coupling (SC) approximation, that is, in isolation from other modes, which relies on the assumption that radial modes do not resonate with other modes. However, it is well known that modes, including radial modes, do cross-couple (i.e. resonate) with other modes, in particular when the two modes have similar frequency (e.g. Deuss & Woodhouse 2001; Irving *et al.* 2008). Here, we will take cross-coupling between radial and nearby modes into account. Prior to our study, Laske *et al.* (2001) published a brief abstract where they also allow cross-coupling in radial modes measurements, however they only reported the effect on their centre frequency measurements. They found that when radial modes are allowed to couple, their centre frequencies shift towards values closer to Preliminary Reference Earth Model (PREM, Dziewonski & Anderson 1981). They speculated that previous studies may have mistakenly reported measurements of modes coupling to radial modes, as the actual radial mode.

We will show that radial modes may provide us with improved constraints on inner core anisotropy. Radial modes most strongly cross-couple to their closest inner core sensitive spheroidal mode (PKIKP equivalent modes), both through ellipticity and inner core anisotropy (Irving *et al.* 2008). Cylindrical anisotropy is a well-known property of the inner core, with the fast axis roughly aligned to the axis of rotation (Woodhouse *et al.* 1986; Tromp 1993; He & Tromp 1996; Durek & Romanowicz 1999; Beghein & Trampert 2003; Deuss *et al.* 2010, 2013; Mäkinen & Deuss 2013). Much less is known about radial anisotropy in the inner core; only one recent study has shown that the centre frequencies of radial modes may be able to constrain radial inner core anisotropy (Lythgoe & Deuss 2015).

Here, we will significantly increase the amount of data used to observe radial modes and take cross-coupling to nearby modes into account. We will show that including cross-coupling in our normal mode measurements improves the fit between data and synthetics, and gives better centre frequency and attenuation estimates of radial modes, as well as provides us with new constraints on inner core radial and cylindrical anisotropy.

2 THEORETICAL BACKGROUND AND METHOD

Normal modes are standing waves along the radius and surface of our planet, that only exist for discrete frequencies. There are two types: toroidal modes ${}_nT_l$, which consist of *SH* motion, and spheroidal modes ${}_nS_l$, which consist of *P–SV* motion. Both mode types are characterized by two numbers, the angular order l and the overtone number n. The overtone number is related to the radial pattern, and the angular order to the number of nodal lines over the Earth's surface. Radial modes ${}_nS_0$, are a special subset of spheroidal modes. These modes have $l = 0$ and no nodal lines over the Earth's surface. They describe the radial expansion and contraction of the whole Earth. Here, we will concentrate on measuring radial modes and their coupling to $l = 2$ spheroidal modes, ${}_nS_2$.

Table 1. Earthquakes catalogue for radial modes. The date format is day/month/year, depth is in km, M_w is the moment magnitude as listed in the CMT catalogue and N_s is the number of stations available per event.

Date	Location	Depth	M_w	N_s
30/05/15	Bonin Islands, Japan	681.0	7.9	76
24/05/13	Sea of Okhotsk	611.0	8.3	105
11/03/11	Tohoku, Japan	29.0	9.1	139
27/02/10	Chile	23.2	8.8	129
05/07/08	Sea of Okhotsk	615.2	7.7	64
13/01/07	Kuril Islands	12.0	8.1	58
15/11/06	Kuril Islands	13.5	8.3	69
03/05/06	Tonga Islands	67.8	8.0	43
28/03/05	Northern Sumatra	25.8	8.6	91
23/06/01	Coast of Peru	29.6	8.4	88
25/03/98	Balleny Islands	28.8	8.1	66
17/06/96	Flores Sea	584.2	7.8	53
30/07/95	Northern Chile	28.7	8.0	50
04/10/94	Kuril Islands	68.2	8.3	46
09/06/94	Bolivia	647.1	8.3	56
09/03/94	Fiji Islands	567.8	7.6	54

Each normal mode is a multiplet consisting of $2l + 1$ singlets. In a spherical, non-rotating, elastic, isotropic Earth the $2l + 1$ singlets are degenerate, meaning they all have the same frequency. This degeneracy is removed by the effects of rotation, ellipticity, anisotropy and lateral heterogeneities, which we call splitting. We calculate splitting through perturbation theory (Dahlen 1968; Woodhouse & Dahlen 1978; Woodhouse 1980). This calculation can either be done using (i) the SC approximation, were modes are treated as isolated; (ii) the group-coupling (GC) approximation, which includes the cross-coupling between two or more modes close in frequency; or (iii) full-coupling (FC), were cross-coupling between all modes in a certain frequency band is included (Deuss & Woodhouse 2001).

Radial modes with $l = 0$ consist of only one singlet and therefore have been considered not to be sensitive to 3-D structure. However, this is only true when radial modes are studied using the SC approximation. In SC, a mode is sensitive to structure of degree $s = 2l$, which means radial modes are only sensitive to $s = 0$ structure. Radial modes do become sensitive to 3-D structure when they are cross-coupled to other modes. In GC, two spheroidal modes with angular orders l and l' are sensitive to $|l - l'| \leq s \leq |l + l'|$ structure. Thus, a radial mode ${}_nS_0$ will couple with a spheroidal mode ${}_nS_{l'}$ for structure with $s = l'$. Radial modes most strongly couple with other spheroidal modes with $l' = 2$, and thus $s = 2$ structure, which includes inner core anisotropy and ellipticity. Although these $l' = 2$ modes can be up to 0.1 mHz away from the radial modes, the strong interactions between them produce wide band cross-coupling, meaning strong coupling between modes that are not so close in frequency. Here, we make measurements of radial modes in SC and GC, and consider FC a second-order effect.

We will use the generalized splitting function approach of Resovsky & Ritzwoller (1998) to measure normal mode splitting both in SC and GC, following the method explained and applied in Deuss *et al.* (2013). Splitting functions are depth-averaged models of how one particular mode 'sees' the Earth (Woodhouse & Giardini 1985). They are linearly dependent on heterogeneous and anisotropic structure, and for this reason can be easily incorporated by other scientists in tomographic modelling inversions (e.g. Ritsema *et al.* 1999, 2011; Moulik & Ekström 2014; Koelemeijer *et al.* 2016). Splitting function coefficients c_{st} are used to calculate the

Table 2. Selected time window compared to theoretical 1.1 Q cycle for all inverted radial modes, both in hours. Also listed: the $l = 2$ mode pair of each radial mode and its sensitivity type, and distance in mHz between them.

Radial mode	1.1 Q cycle	Time window	$l = 2$ mode	$l = 2$ type	Distance mHz
${}_0S_0$	1996	5-2000	${}_2S_2$	IC	0.124
${}_1S_0$	281	5-280	${}_4S_2$	v_p	0.091
${}_2S_0$	151	5-150	${}_7S_2$	IC	0.007
${}_3S_0$	101	35-105	${}_8S_2$, ${}_9S_2$	IC	0.057, 0.039
${}_4S_0$	72	25-100	${}_{10}S_2$, ${}_{11}S_2$	IC	0.073, 0.047
${}_5S_0$	58	35-90	${}_{13}S_2$	IC	0.039
${}_6S_0$	49	20-75	${}_{16}S_2$	IC	0.043
${}_7S_0$	41	10-65	${}_{18}S_2$	IC	0.035
${}_8S_0$	35	10-55	${}_{20}S_2$	IC	0.067
${}_9S_0$	31	10-50	${}_{22}S_2$	IC	0.056
${}_{11}S_0$	26	8-50	${}_{27}S_2$	IC	0.023

splitting matrix, that together with the effects of the 1-D reference model (Dziewonski & Anderson 1981), ellipticity and rotation allow us to calculate synthetic seismograms, which are then compared to earthquake data (Deuss & Woodhouse 2001; Deuss *et al.* 2013). The splitting function coefficients are written as

$$c_{st} = \int_0^a \delta m_{st}(r) \cdot K_s(r)\, dr + \sum_d \delta h^d_{st}\, H^d_s \tag{1}$$

where s is the angular order and t the azimuthal order of the Earth's structure, and the integral is calculated over a, the radius of the Earth. $K_s(r)$ and H^d_s are known kernels (Woodhouse 1980); δm_{st} are the coefficients of the Earth's structure (compressional and shear wave velocity v_p, v_s; density ρ) and δh^d_{st} are the coefficients of discontinuity topography. Both δm_{st} and δh^d_{st} can be determined in a linear inversion using the measured splitting function coefficients and the known sensitivity kernels. Splitting function coefficients are usually visualized in a map $F(\theta, \phi)$, comparable to phase-velocity maps used in surface wave analysis. These maps show regional frequency variations of a specific normal mode, and are calculated using

$$F(\theta, \phi) = \sum_{s=2}^{2l} \sum_{t=-s}^{s} Y^t_s(\theta, \phi)\, c_{st} \tag{2}$$

where $Y^t_s(\theta, \phi)$ are the fully normalized complex spherical harmonics (Edmonds 1960) and (θ, ϕ) indicate the surface position. Splitting function measurements also provide constraints on the average 1-D structure seen by a mode. $\mathrm{Re}(c_{00})$ is related to the shift in centre frequency f_c, and $\mathrm{Im}(c_{00})$ is related to the shift in the quality factor Q

$$f_c = f_0 + (4\pi)^{-1/2}\, \mathrm{Re}(c_{00}) \tag{3}$$

$$Q = \frac{f_c}{2\left(\frac{f_0}{2Q_0} + (4\pi)^{-1/2}\, \mathrm{Im}(c_{00})\right)} \tag{4}$$

where f_0 and Q_0 are the reference model frequency and quality factor. Radial modes are defined only by $\mathrm{Re}(c_{00})$ and $\mathrm{Im}(c_{00})$, and solely provide constrains on the Earth's 1-D structure. However, their coupling with other modes allows us to measure 3-D structure as well.

The inversion scheme used is the iterated least-squares method of Tarantola & Valette (1982), following the same iterative spectral fitting method as Deuss *et al.* (2013). We define the misfit m between the data $\mathbf{d}_i$ and the synthetics $\mathbf{u}_i(c_{st})$ as

$$m = \frac{1}{N} \sum^{N} \frac{\sum_{i=1}^{n} (\mathbf{d}_i - \mathbf{u}_i(c_{st}))^2}{\sum_{i=1}^{n} (\mathbf{d}_i)^2} \tag{5}$$

where is N is the total number of spectral segments for a specific mode and n are the number of data points contained within each spectral segment.

Unlike Pachhai *et al.* (2020), who use the autoregressive matrix method together with a Bayesian inversion and Metropolis–Hasting Sampling in order to obtain the probabilistic distributions of their measurements, we calculate the uncertainties of our measurements by doing event cross-validation. We do this by removing whole events at the time (e.g. 1994 Bolivia or 2011 Tohoku events), including all stations, and measure what the splitting function would be without this event. In this way, we estimate earthquake bias (e.g. Deuss *et al.* 2013). In addition, from the results of radial modes synthetic tests, we include the GC Q value deviations from the synthetic input in the Q value uncertainties of radial modes (Fig. S1, Supporting Information).

All mantle splitting function predictions computed here use the shear velocity model S20RTS (Ritsema *et al.* 1999), with a scaling of the form $\delta v_p/v_p = 0.5\, \delta v_s/v_s$ and $\delta\rho/\rho = 0.3\, \delta v_s/v_s$, together with the crustal structure model CRUST5.1 (Mooney *et al.* 1998). Inner core anisotropy is included using the model Tromp (1993).

3 DATA

Normal mode observations require several day-long seismic data of large earthquakes ($M_w > 7.4$) with a high signal-to-noise ratio (ideally above 2), to make their discrete frequencies visible as

Table 3. Misfit comparison of the SC and GC approach to previous measurements. Misfits for: PREM (m^{P}); REM website (m^{REM}, Laske *et al.* 2005); He & Tromp (1996) (m^{HT}) and our measurements (m^{SC}, m^{GC}). Number of events N_{ev} and number of stations N_s are listed both for the radial modes and $l = 2$ modes spectral data. All misfit calculations include the effects of rotation and ellipticity.

	N_s	N_{ev}	m^{P}	m^{REM}	m^{HT}	m^{SC}	m^{GC}		N_s	N_{ev}	m^{GC}
${}_0S_0$	25	5	1.59	2.58	–	0.04	0.04	${}_2S_2$	–	–	–
${}_1S_0$	224	9	0.32	0.29	0.14	0.082	0.081	${}_4S_2$	1537	90	0.31
${}_2S_0$-${}_7S_2$	300	9	2.46	0.82	2.74	0.38	0.13				
${}_3S_0$	139	5	1.59	0.45	0.45	0.44	0.37	${}_8S_2$-${}_9S_2$	740	57	0.34
${}_4S_0$	428	11	0.62	0.54	0.55	0.55	0.51	${}_{10}S_2$-${}_{11}S_2$	1320	58	0.33
${}_5S_0$	146	5	0.93	0.32	0.46	0.23	0.21	${}_{13}S_2$	700	37	0.14
${}_6S_0$	134	5	1.65	0.17	0.23	0.16	0.16	${}_{16}S_2$	–	–	–
${}_7S_0$	68	3	1.90	0.56	–	0.37	0.24	${}_{18}S_2$	–	–	–
${}_8S_0$	58	9	1.11	0.78	0.73	0.67	0.64	${}_{20}S_2$	–	–	–
${}_9S_0$	376	14	1.99	1.15	0.99	0.39	0.36	${}_{22}S_2$	–	–	–
${}_{11}S_0$-${}_{27}S_2$	355	23	1.72	–	–	–	0.29				

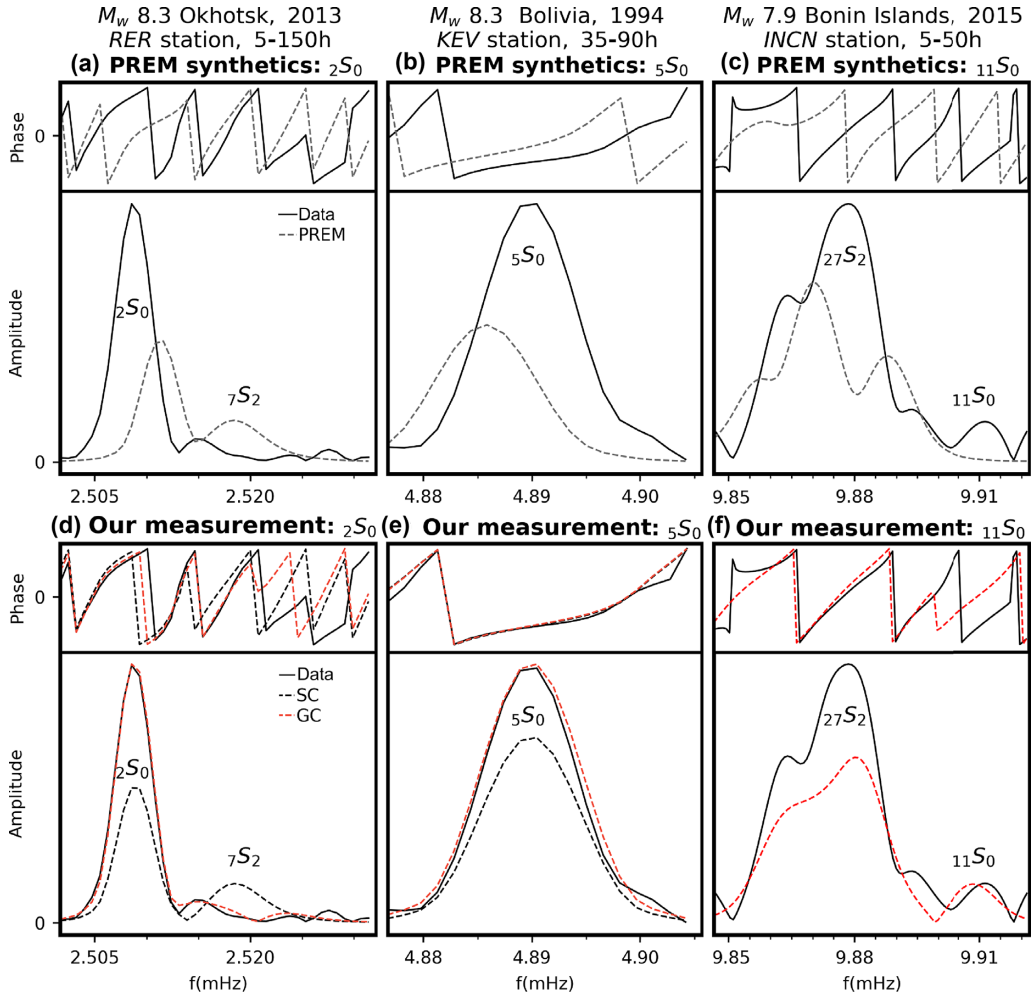

Figure 1. Amplitude and phase spectra for radial modes $_2S_0$-$_7S_2$, $_5S_0$ and $_{11}S_0$-$_{27}S_2$. Data compared to (a)–(c) 1-D PREM synthetics together with rotation and ellipticity and no cross-coupling, and (d)–(f) our SC and GC measurements. The frequency window showed for $_2S_0$-$_7S_2$ and $_{11}S_0$-$_{27}S_2$ is extended beyond our selected frequency window for the inversion. Mode $_{13}S_2$ is not shown as it has both a different selected time and frequency window as $_5S_0$.

distinct peaks in the frequency spectrum. Radial modes are most strongly exited by the largest and deepest events; they have very long periods and are only slowly attenuating, thus requiring week-long data. Here, we will use 16 of the largest events available in the last 25 yr (given in Table 1) to invert for radial modes $_0S_0$ up to $_{11}S_0$. We are including two new events compared to the events used in Deuss *et al.* (2013) and Koelemeijer *et al.* (2013), and excluding the 2004 great Sumatra earthquake due to its complicated moment tensor solution. The influence of this earthquake was most notorious for mode $_0S_0$, with this event requiring a different solution for Q than other earthquakes. Although the effect was minimum for modes with $n > 0$, we decided to exclude this earthquake from our final measurements. There could also be an influence of the chosen networks and stations on our measurements (Majstorović *et al.* 2019). We did not see any evidence for network problems, but for comparison all stations and networks used in our study are given in Table S1 in the Supporting Information.

In order to invert for the lowest radial order and most weakly attenuating radial modes, the time window was expanded to 83 days for $_0S_0$ and to 13 days for $_1S_0$, $_2S_0$. Our new data set was treated using the same steps as Deuss *et al.* (2013), and includes only vertical component data as no high signal-to-noise horizontal component data is available for the radial and spheroidal modes measured in this study.

To select the data's time windows we used each mode's Q-cycle as a reference (Dahlen 1982). The Q-cycle is defined as the time necessary for a wave to decay to $e^{-\pi}$ of its original amplitude. This is specially important for radial modes, because if not enough hours are included, we cannot find a solution that satisfies the data at all time windows. A time window end-time lower than the Q-cycle will affect the measured centre frequency and specially the Q value. In addition, the first tens of hours were excluded for all modes, in order to remove the effect of strongly attenuating modes with similar frequencies, but much smaller Q-cycles. The exact time windows used for every mode are listed in Table 2. The selected time-series was then padded with zeros to the next power of 2 and Fourier transformed to obtain spectral data in the frequency domain. All generated synthetic data are processed in the same way as the real data, following the same steps outlined by Deuss *et al.* (2013).

The selection of the radial modes segments was conducted through visual inspection. We have taken the spectral segments for the $l = 2$ spheroidal modes from the extended event catalogue of Deuss *et al.* (2013), and added spectra for two more recent events. For our GC inversions, we used two separate time windows and

Table 4. Radial modes measurements of centre frequencies f_c (μHz) and Q in SC and GC. PREM centre frequency f_0 (μHz) and quality factor Q_0 are also given.

	f_0	f_c^{SC}	f_c^{GC}	Q_0	Q^{SC}	Q^{GC}
${}_0S_0$	814.31	$814.60^{+0.0007}_{-0.0014}$	$814.60^{+0.0007}_{-0.0014}$	5327	5982^{+211}_{-174}	5982^{+211}_{-174}
${}_1S_0$	1631.34	$1631.55^{+0.004}_{-0.01}$	$1631.56^{+0.02}_{-0.12}$	1499	1849^{+7}_{-20}	1856^{+144}_{-143}
${}_2S_0$	2510.48	$2508.45^{+0.06}_{-0.08}$	$2509.30^{+0.14}_{-0.22}$	1242	1241^{+97}_{-68}	1788^{+117}_{-122}
${}_3S_0$	3271.18	$3272.40^{+0.06}_{-0.04}$	$3271.98^{+0.06}_{-0.04}$	1083	1222^{+75}_{-22}	1242^{+80}_{-46}
${}_4S_0$	4105.76	$4106.51^{+0.05}_{-0.12}$	$4105.99^{+0.03}_{-0.41}$	969	1157^{+86}_{-31}	1176^{+109}_{-33}
${}_5S_0$	4884.17	$4888.34^{+0.04}_{-0.03}$	$4886.72^{+0.19}_{-0.16}$	921	1016^{+31}_{-11}	1008^{+11}_{-13}
${}_6S_0$	5740.25	$5742.24^{+0.09}_{-0.05}$	$5742.11^{+0.007}_{-0.57}$	913	1086^{+52}_{-32}	1077^{+111}_{-34}
${}_7S_0$	6580.71	$6586.58^{+0.29}_{-0.54}$	$6583.56^{+0.55}_{-0.13}$	881	1035^{+132}_{-47}	883^{+87}_{-66}
${}_8S_0$	7424.13	$7430.30^{+0.16}_{-0.40}$	$7429.66^{+0.14}_{-0.40}$	852	1305^{+1}_{-223}	1198^{+139}_{-45}
${}_9S_0$	8262.64	$8270.01^{+0.11}_{-0.11}$	$8268.27^{+0.25}_{-0.21}$	840	933^{+51}_{-28}	965^{+63}_{-46}
${}_{11}S_0$	9865.33	–	$9893.37^{+0.004}_{-0.35}$	832	–	1053^{+93}_{-1}

frequency windows for the spectral segments, one for the radial mode and one for the $l = 2$ mode, with the exception of the mode pairs ${}_2S_0$-${}_7S_2$ and ${}_{11}S_0$-${}_{27}S_2$. The time windows used for the radial modes are listed in Table 2, the time windows used for the $l = 2$ modes are the ones selected by Deuss *et al.* (2013). The reasons for using different spectral segments for radial and $l = 2$ modes are: (i) the large difference in frequency between the two types of modes (Table 2), which are so far away from each other in frequency that many other modes lie in between them; (ii) radial modes and $l = 2$ modes have different Q cycles and (iii) $l = 2$ modes usually lie in the same frequency window as other strongly attenuating modes.

Overall, our new data set has a factor of 10 increase in data size when compared to previous studies (Widmer *et al.* 1991; Durek & Ekström 1995; He & Tromp 1996). We include between 3 and 14 earthquakes in each of our radial modes measurements (see Table 3), whereas studies before only used one or two events.

4 RESULTS

We first use our new data set to measure radial modes using the SC approximation, which allows us to compare our measurements to previous studies (see Section 4.1). Next, we include GC to nearby $l = 2$ modes to investigate the influence of coupling on the measured centre frequency f_c and quality factor Q (see Section 4.2). Finally, we interpret our f_c measurements to obtain new constraints on inner core anisotropy and 1-D bulk attenuation (see Section 5).

4.1 Self-coupling approach

We first measured radial modes ${}_0S_0$ up to ${}_9S_0$ in the SC approach. ${}_{10}S_0$ was not measured because of its low spectral amplitude and the presence of too many overriding nearby modes. ${}_{11}S_0$ could not be measured using SC, because of its close proximity to mode ${}_{27}S_2$ and its significant amplitude difference with this mode. For modes ${}_0S_0$, ${}_2S_0$, ${}_5S_0$, ${}_7S_0$, ${}_8S_0$, ${}_9S_0$ and ${}_{11}S_0$, it was necessary to start from a given centre frequency shift, which we determined by visually inspecting the data. This step, which was also necessary when conducting synthetics tests, is needed when PREM's predictions lie too far away from the data (Figs 1a–c), and given that we use only small steps in our iterated nonlinear inversion, we need to use a starting model that moves in the right direction. For all other radial modes, inversions were started from PREM.

Our measured centre frequency and quality factor values are shown in Table 4. Fig. 1 displays normal mode spectra for radial modes ${}_2S_0$ and ${}_5S_0$, showing the fit between the observed data, PREM synthetics and synthetics calculated using our f_c^{SC} and Q^{SC} values measured in the SC approximation. In these individual spectra, we see that our SC measurements improve the data fit compared to the PREM synthetics. Table 3 shows that for our whole data set, the SC misfit is better than the PREM misfit. For comparison, the misfit using centre frequency and quality factor values from previous studies are also included (He & Tromp (1996) and the Reference Earth Model webpage (REM, Laske *et al.* 2005)). Again, we see that our values have the lowest misfit.

We compare our f_c and Q measurements and their uncertainties to PREM (Fig. 2), and against the measurements from previous studies (Widmer *et al.* 1991; Durek & Ekström 1995; He & Tromp 1996; Laske *et al.* 2005). Our SC results agree with these studies, which only used the SC approach, especially the f_c values are very similar. This implies that the f_c measurements are very robust, and can be derived even with the limited data used in previous studies. On the other hand, much larger variation is seen in the quality factor Q between the different studies. For modes ${}_5S_0$ and ${}_9S_0$, we obtain lower Q values. The other radial modes are within the Q error bars of previous measurements. Although the Q measurement of mode ${}_0S_0$ falls within the error bars given by previous measurements, we do measure a significantly higher Q value than before.

4.2 Group-coupling approach

4.2.1 Radial modes

Next, we include GC in our measurements. Radial modes have their strongest cross-coupling with $l = 2$ inner core sensitive spheroidal modes, with differences in frequency between the cross-coupled modes of up to 0.124 mHz (Table 2). Fig. 3 shows the sensitivity kernels as a function of depth for the radial and $l = 2$ spheroidal modes. Radial modes (Fig. 3a) are mostly sensitive to compressional velocity (v_p), while about half of the corresponding $l = 2$ modes (Fig. 3b), are more strongly sensitive to shear velocity (v_s) in the mantle and the inner core. The $l = 2$ modes with the highest overtone numbers (${}_{18}S_2$ up to ${}_{27}S_2$) do have dominant sensitivity to compressional velocity v_p and have sensitivity kernels which are much more similar to the radial modes. The majority of the $l = 2$ spheroidal modes are sensitive to the inner core, and they couple with radial

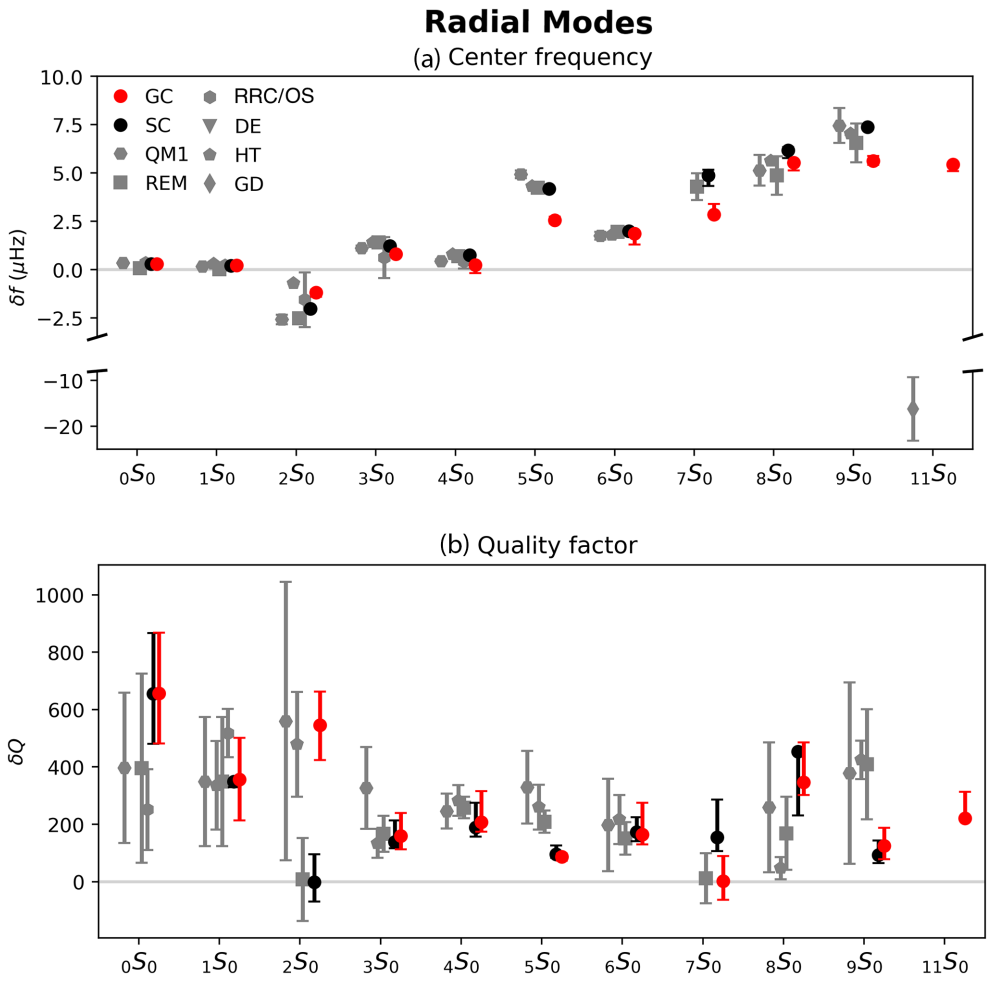

Figure 2. Radial modes measurements with respect to PREM. f_c and Q shifts are compared to previous observations in grey. SC: our self-coupling measurements (black), GC: our group-coupling measurements (red), GD: Gilbert & Dziewonski (1975), HT: He & Tromp (1996), QM1: observations used in Widmer *et al.* (1991), REM: Reference Earth Model website, DE: observations used in Durek & Ekström (1995), RRC: Roult *et al.* (2010), which only measured δf_c in (a), and OS: Okal & Stein (2009), which only measured δQ in (b).

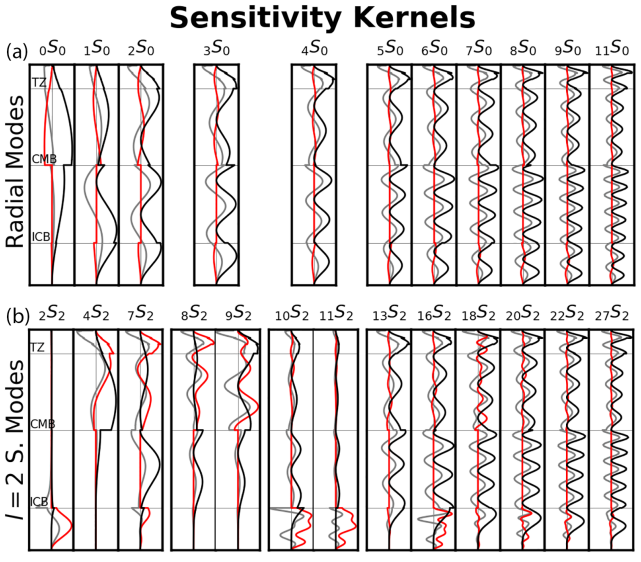

Figure 3. Depth sensitivity kernels of density in grey (ρ), shear velocity in red (v_s) and compressional velocity in black (v_p), calculated from PREM. For (a) radial modes and (b) $l = 2$ modes coupling to radial modes. Transition zone (TZ), core–mantle boundary (CMB) and ICB marked in figure.

modes for ellipticity and inner core cylindrical anisotropy, which are both degree $s = 2$ structure.

In order to validate our GC results, we conducted tests in which we measure radial and $l = 2$ mode pairs both in SC and GC using synthetic data. In these tests, we are able to recover the synthetic cross-coupling structure between the mode pairs. Similarly, when cross-coupling is not present in the synthetic data, but is included in the splitting function measurement, we do not recover cross-coupling structure. ${}_0S_0$ is the only mode where it was not possible to recover synthetic cross-coupling structure, which we also observe using our real data. Following the same strategy used for all other mode pairs and described in Section 2, we attempted to measure mode ${}_0S_0$ in GC with modes ${}_2S_2$, ${}_1S_2$ and ${}_0S_5$, which Rosat *et al.* (2007) showed cross-couple strongly with ${}_0S_0$. However, in all cases we were unable to measure their cross-coupling using our technique. This is especially evident in tests where cross-coupling was included in the synthetics, but still we were not able to retrieve it in the splitting function measurement (Fig. S2, Supporting Information). In addition to the large frequency distance between these mode pairs (> 0.124 mHz), the reason for this is most likely that modes ${}_2S_2$, ${}_1S_2$ and ${}_0S_5$ have a much smaller Q than ${}_0S_0$, and therefore decay much faster and are not visible any more after one or two days, while 83 days are required to properly measure ${}_0S_0$. For modes

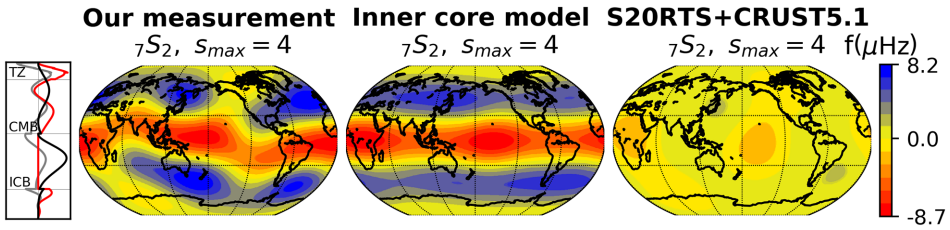

Figure 4. Splitting function measurement of mode $_7S_2$, measured in GC with $_2S_0$, compared to a combined mantle and inner core prediction (middle) and a mantle prediction (right). Inner core model: Woodhouse *et al.* (1986).

with $n > 0$ (Fig. S1, Supporting Information), we observe a strong trade-off between the cross-coupling c_{20} coefficient (i.e. degree 2 structure) and the radial modes' splitting function coefficient Re(c_{00}) (i.e. the centre frequency), but not with Im(c_{00}) (i.e. the quality factor Q). We see the same effect in our measurements using real data, which we will explain in detail in this section.

All the modes measured in SC (Section 4.1), are here measured again in GC, with the addition of $_{11}S_0$-$_{27}S_2$ (Figs 1c and f). Radial mode $_3S_0$ cross-couples to $_8S_2$-$_9S_2$, and $_4S_0$ cross-couples to $_{10}S_2$-$_{11}S_2$. These $l = 2$ modes are pairs of inner core sensitive modes, which have almost identical frequency and are very strongly coupled for structure up to degree 4. They also cross-couple to their respective radial mode for degree-two structure. Andrews *et al.* (2006), performed synthetic tests on these mode pairs which are of the type $_{n\pm1}S_2$-$_nS_2$, and found that they are strongly coupled by 1-D attenuation. In the case of $_{10}S_2$-$_{11}S_2$, which strongly depends on the underlying 1-D model used, the cross-coupling causes $_{10}S_2$ to increase its Q value significantly, which allows it to be visible in the spectra. The $_{n\pm1}S_2$-$_nS_2$ modes used here were first measured in pairs (see Talavera-Soza & Deuss 2020), and those results have been used as a starting model here in our GC measurements.

All radial modes and their $l = 2$ spheroidal modes have been cross-coupled for ellipticity as predicted by PREM. In the case of modes $_0S_0$, $_6S_0$, $_7S_0$, $_8S_0$, $_9S_0$, we are unable to robustly constrain additional cross-coupling for $s = 2$ structure to their corresponding $l = 2$ modes. These radial modes couple to $_2S_2$, $_{16}S_2$, $_{18}S_2$, $_{20}S_2$, $_{22}S_2$ respectively, none of which can be measured, either because they are not visible in the data (inner core confined modes) or their visibility is so poor that not enough normal-mode spectra were available to obtain a stable measurement. Radial modes $_1S_0$, $_2S_0$, $_3S_0$, $_4S_0$, $_5S_0$ and $_{11}S_0$ were all cross-coupled for $s = 2$ structure because enough spectra were available for their corresponding $l = 2$ modes.

Fig. 2(a) shows our f_c and Q measurements along the radial mode branch as a function of overtone number n. We observe smoother variations in centre frequency f_c in our GC than in our SC measurements; modes $_2S_0$ and $_5S_0$ are outliers in the SC measurements and move towards a smoother variation along the branch in the GC measurements. Thus, including GC results in a much improved branch consistency between all radial mode f_c measurements. The cross-coupling effect on the modes becomes larger as we move to higher frequencies along the radial branch, which is evidenced when comparing the SC and GC misfits (Table 3). For example, the measured cross-coupling of $_1S_0$-$_4S_2$ is not as strong as the one exhibited by other mode pairs at higher frequencies. This is reflected both in the amplitude of the f_c shift and, as we will see later, also in the size of the cross-coupled splitting function anomalies.

In the past, Laske *et al.* (2001) explored the effect of cross-coupling on radial modes, and reported that it produces an overall f_c shift towards values closer to PREM. We observe a similar behaviour, but not as pronounced as the one outlined in the Laske *et al.* (2001) abstract. Unfortunately, we are not able to directly compare Laske *et al.* (2001) abstract results to our measurements. But, we do distinguish a systematic shift of the f_c towards PREM, as we allow the radial modes to couple with their closest $l = 2$ modes. This is notable even when just ellipticity is included in GC, but is more evident when we allow cross-coupling for all degree-two structure, as the f_c shift is affected by both, as is the case of $_2S_0$, $_5S_0$ and $_7S_0$ (Fig. 2a).

As seen in the synthetic tests, the quality factor Q, on the other hand, shows no clear pattern for all modes, and sometimes is not affected at all by the cross-coupling (Fig. 2b). The effect of cross-coupling on Q, is only evident when the GC modes are very close

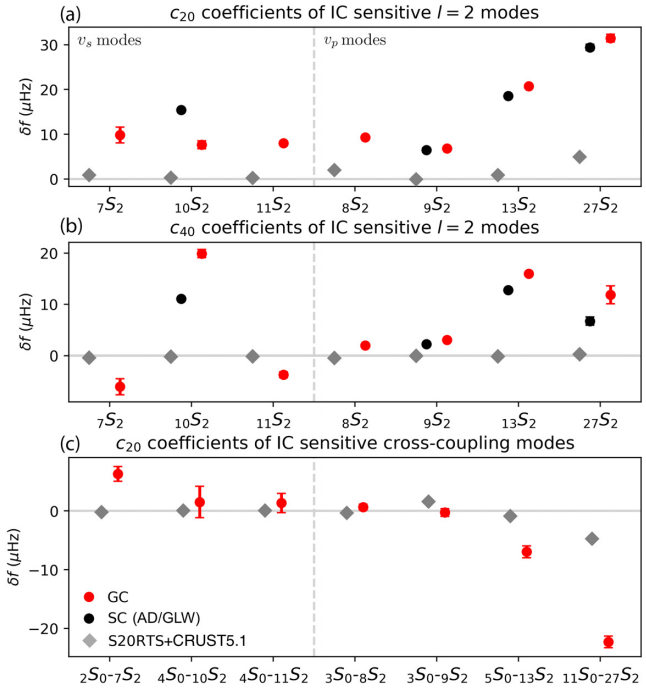

Figure 5. c_{20} and c_{40} splitting function coefficients for (a) and (b) $l = 2$ modes sensitive to the inner core and (c) their corresponding cross-coupling to radial modes. Our GC measurements (red) are compare to model predictions and previous measurements. S20RTS: mantle model with crustal corrections (light grey); Inner core (IC) model: Tromp (1993) (dark grey); measurements in SC (black) by Deuss *et al.* (2013) (AD) and Giardini *et al.* (1988) for $_{10}S_2$ (GLW).

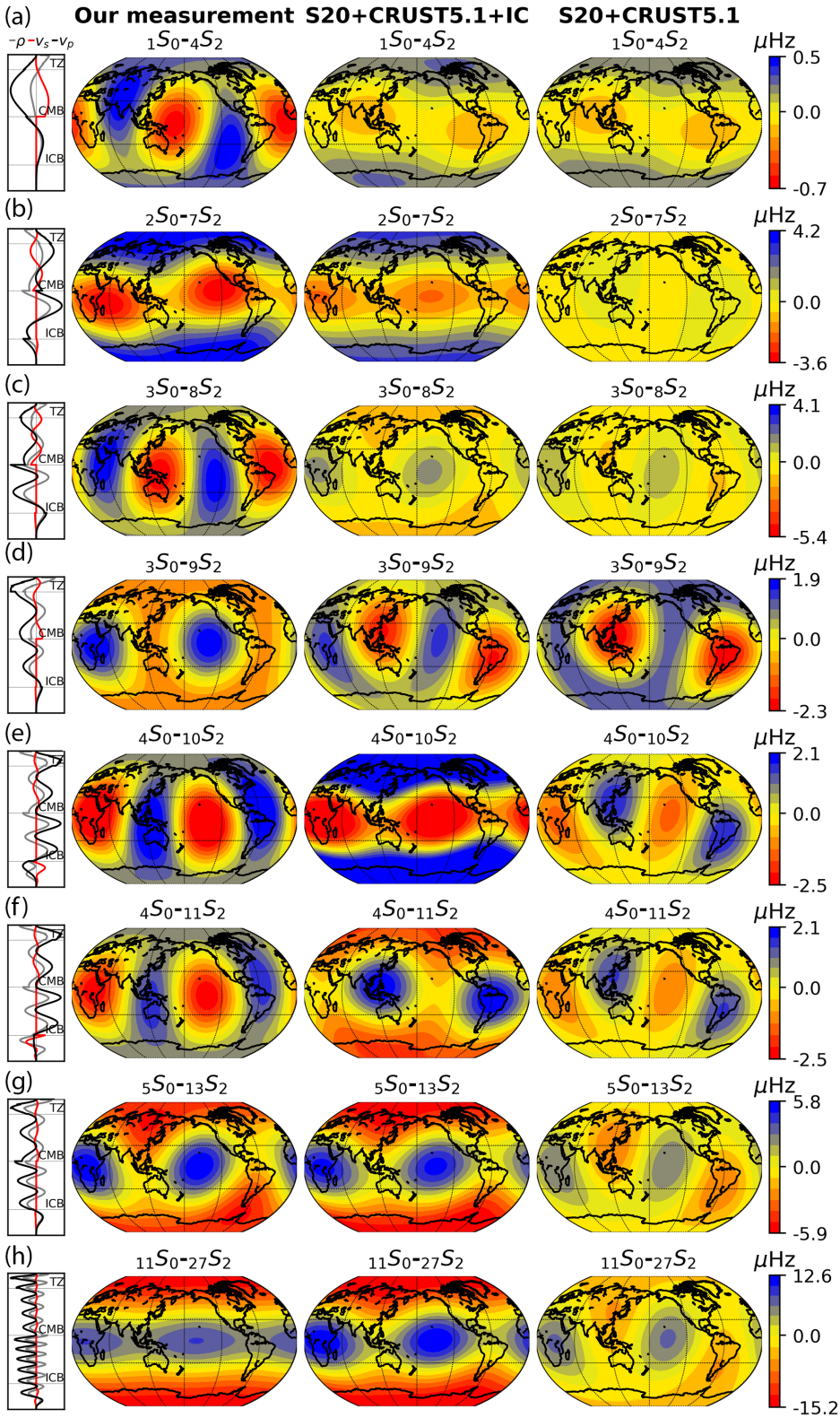

Figure 6. Cross-coupling splitting functions measurements between radial modes and $l = 2$ modes for $s = 2$, compared to a combined mantle and inner core anisotropy model using Tromp (1993, middle) and only a mantle prediction (right).

in frequency, as is the case for modes $_2S_0$-$_7S_2$ which cannot be disentangled. We expect that the strong GC between $_2S_0$-$_7S_2$, is the reason of the contradicting results for $_2S_0$ in previous studies (Fig. 2b).

Measuring GC in our inversions reduces the misfit to the data, specially as radial modes and their corresponding $l = 2$ modes get closer in frequency making their cross-coupling stronger (Fig. 1 and Table 3). However, in some of the cases where cross-coupling could

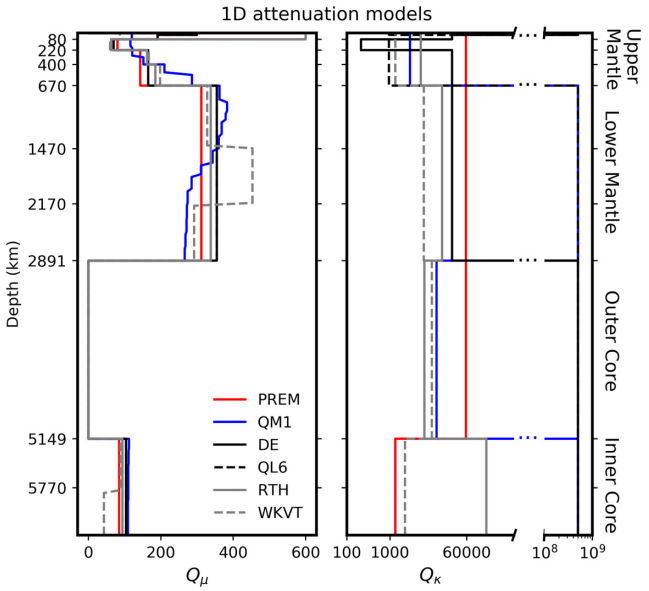

Figure 7. 1-D attenuation models based on normal modes, for shear attenuation Q_μ (left) and bulk attenuation Q_κ (right). Models PREM (Dziewonski & Anderson 1981); QM1 (Widmer *et al.* 1991); DE (Durek & Ekström 1995); QL6 (Durek & Ekström 1996); RTH (Resovsky *et al.* 2005) and WKVT (de Wit *et al.* 2014).

not be robustly measured we see that the misfit remains the same as in the SC case, for example, ${}_0S_0$, ${}_6S_0$. This is to be expected as we attempt to measure cross-coupling between $l = 2$ and radial modes only using data for the radial modes.

4.2.2 $l = 2$ Modes

The cross-coupling also allows us to measure splitting functions for the $l = 2$ modes and their cross-coupled splitting functions with the radial modes. We measured the splitting function coefficients of modes ${}_7S_2$, ${}_8S_2$, ${}_9S_2$, ${}_{10}S_2$, ${}_{11}S_2$, ${}_{13}S_2$ and ${}_{27}S_2$. Fig. 4 shows our splitting function map for mode ${}_7S_2$ which has not been reported before. It shows the typical zonal splitting of an inner core sensitive mode, with strong anomalies along the poles and the equator. The splitting functions of the other $l = 2$ modes show a similar pattern, see Fig. S3 in the Supporting Infomation, where we compare our $l = 2$ observations to Deuss *et al.* (2013), who measured the modes in SC using the same method, and Pachhai *et al.* (2020), who also measured the modes in SC but using the matrix autoregressive analysis method. The anomalous zonal splitting is due to strong zonal degree-two (c_{20}) and degree-four (c_{40}) values (Figs 5a and b). This typical zonal splitting cannot be satisfied by mantle and crustal predictions, and requires inner core cylindrical anisotropy with the fast axis aligned with the rotation axis of the Earth (i.e. Woodhouse *et al.* 1986). Overall, when comparing our GC results for the inner core sensitive modes to previous measurements in SC (Giardini *et al.* 1988; Deuss *et al.* 2013), we find that coefficients c_{20} and c_{40} have higher values when we include cross-coupling.

4.2.3 Cross-coupling

The interpretation of our cross-coupling splitting function maps is not as straightforward as in the SC case. The reason for this is the more complicated nature of their cross-coupling kernels (Fig. 6), which cause the signature of inner core anisotropy in a splitting function to change. There are still strong anomalies near the poles and along the equator (so-called 'zonal splitting'), but the anomalies near the poles are now negative in some cases, which depends on the specific mode pair. This is not only evident in the observations (left-hand column of Fig. 6), but also in the predictions for an inner core anisotropy model with north–south aligned cylindrical inner core anisotropy (middle column of Fig. 6). The model predictions show that for ${}_1S_0$-${}_4S_2$, ${}_2S_0$-${}_7S_2$, ${}_4S_0$-${}_{10}S_2$, ${}_4S_0$-${}_{11}S_2$ the polar anomalies are expected to be positive. For ${}_3S_0$-${}_8S_2$, ${}_3S_0$-${}_9S_2$, ${}_5S_0$-${}_{13}S_2$ and ${}_{11}S_0$-${}_{27}S_2$ the polar anomalies are negative in the model predictions. Also shown for comparison are the models predictions using only a mantle model. Here, no polar anomalies are visible, but again the sign of the anomalies is sometimes opposite to what we usually see for mantle structure (right-hand column of Fig. 6). By comparing the model predictions (right-hand and middle columns) with the real observations (left-hand column), we interpret our observations as being due to inner core or mantle structure and if it has the expected sign for such structure. The fact that our observations do not always agree with the model predictions, means that our observations provide new information which may help to improve future models.

In Fig. 6, we see that just as for our $l = 2$ modes, the cross-coupled splitting function coefficients of ${}_2S_0$-${}_7S_2$, ${}_5S_0$-${}_{13}S_2$ and ${}_{11}S_0$-${}_{27}S_2$ also show anomalous splitting due to inner core cylindrical anisotropy, as further seen in the c_{20} cross-coupling coefficients in Fig. 5(c). Inner core model predictions of c_{20} cross-coupling coefficients follow the same trend as our observations, with mode pairs ${}_2S_0$-${}_7S_2$, ${}_5S_0$-${}_{13}S_2$ and ${}_{11}S_0$-${}_{27}S_2$ predicted to be strongly sensitive to inner core anisotropy. In spite of also being sensitive to the inner core, the cross-coupled splitting functions of ${}_1S_0$-${}_4S_2$, ${}_3S_0$-${}_8S_2$, ${}_3S_0$-${}_9S_2$, ${}_4S_0$-${}_{10}S_2$ and ${}_4S_0$-${}_{11}S_2$ are dominated by mantle structure, and do not show anomalous zonal splitting near the poles.

5 INTERPRETATION

5.1 Bulk attenuation

The location and strength of bulk attenuation Q_κ inside the Earth has been highly debated, because the observed Q values of radial modes cannot be explained without the presence of finite Q_κ somewhere in the Earth. In the past (see Fig. 7), finite Q_κ has been placed in the upper mantle (Sailor & Dziewonski 1978; Widmer *et al.* 1991; Durek & Ekström 1996), the lithosphere (Durek & Ekström 1995), the inner core (Anderson & Hart 1978; Dziewonski & Anderson 1981) and even the outer core or lower mantle (Resovsky *et al.* 2005; de Wit *et al.* 2014). We calculate Q value predictions for radial modes using a range of 1-D Q_κ profiles, and compare these with our new Q measurements (Fig. 8). We do this by recalculating the mode catalogue for the different 1-D Q_κ profiles using MINEOS (Woodhouse 1988), while keeping the values of v_s, v_p, ρ and Q_μ as in PREM. Mode ${}_0S_0$ is the most sensitive to variations in Q_κ (see Fig. S4, Supporting Information), because it is dominated by compressional energy. Other modes exhibit smaller Q changes as a result of varying Q_κ, specially as we move towards higher frequencies.

We build synthetic 1-D Q_κ profiles by systematically varying the strength of Q_κ in the lithosphere, upper mantle, lower mantle, outer core and inner core, one region at a time, while assuming negligible bulk attenuation elsewhere ($Q_\kappa = 5^8$) and using PREM's 1-D shear attenuation Q_μ profile. We confirm that, as seen in previous probabilistic studies (Resovsky *et al.* 2005; de Wit *et al.* 2014), Q_κ can be placed in different regions of the Earth and yield similar results (Fig. 8). Setting Q_κ to 1200 in the inner core cannot explain the

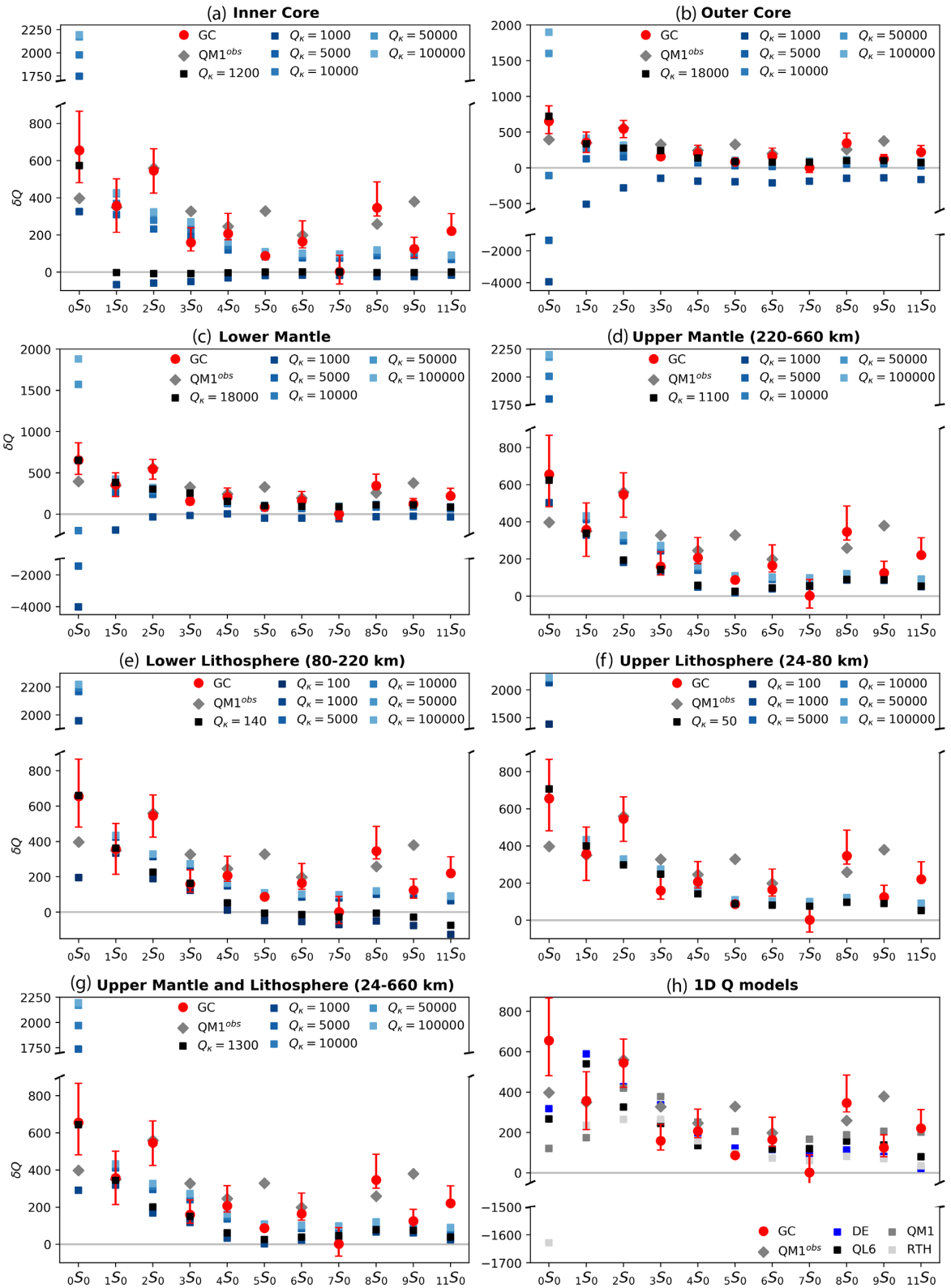

Figure 8. Comparison between 1-D Q model predictions and our GC measurements (red circles), all with respect to PREM. In grey diamonds, the radial mode observations used in model QM1^{obs} (Widmer *et al.* 1991). In (a)–(g), Q_κ is varied in each region, while maintaining Q_κ at 5^8 in all other regions. The blue squares represent the radial modes Q value predictions for each 1-D Q_κ synthetic profile, and the black squares represent the best synthetic predictions in each region. In (h), the 1-D Q model predictions are plotted: DE in blue (Durek & Ekström 1995), QL6 in black (Durek & Ekström 1996), QM1 in dark grey and RTH in light grey (Resovsky *et al.* 2005).

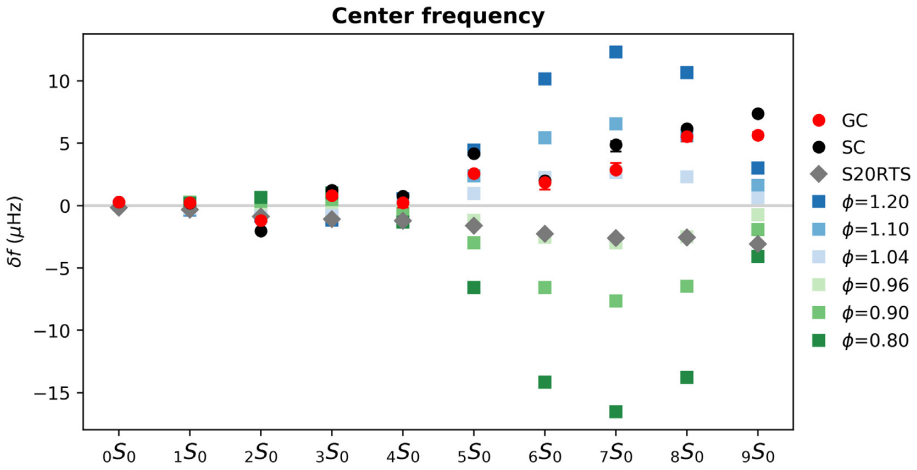

Figure 9. Comparison between f_c predictions obtained by Lythgoe & Deuss (2015) and our SC and GC measurements with respect to PREM. The f_c predictions are obtained by varying the radial anisotropy present in the upper most inner core through the parameter $\phi = v_{pv}^2/v_{ph}^2$, with $v_{pv} < v_{ph}$ in green, $v_{pv} > v_{ph}$ in blue. The PREM line in grey represents no anisotropy and the black markers mantle model S20RTS together with crustal model CRUST5.1.

observations of mode $_0S_0$ and all other radial modes simultaneously (Fig. 8a). PREM does have a comparable value in the inner core (Q_κ=1328), but it is balanced by setting Q_κ=57 822 elsewhere in the Earth. Placing a Q_κ value of 18 000 either in the outer core or lower mantle, gives predictions that agree with all radial modes (Figs 8b and c). This is also the case if we set Q_κ at 1100 in the upper mantle (220–660 km, Fig. 8d). On the other hand, setting Q_κ to 140 in the lower lithosphere (80–220 km) only matches the radial mode branch up to mode $_3S_0$, while all other radial mode Q values are underpredicted (Fig. 8e). Finally, setting Q_κ to 50 in upper part of the lithosphere (24–80 km) gives the best fit to the whole radial

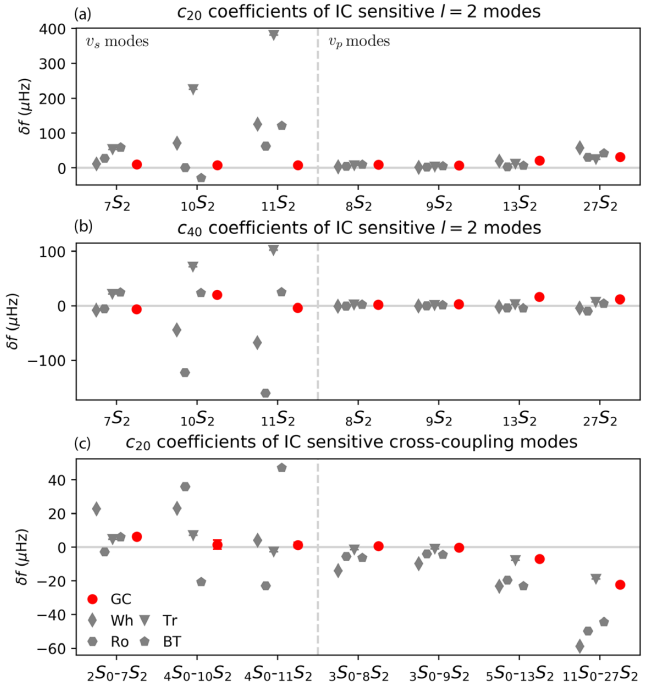

Figure 10. c_{20} and c_{40} splitting function coefficients for (a) and (b) $l = 2$ modes sensitive to the inner core and (c) their corresponding cross-coupling to radial modes. Our GC measurements (red) are compare to inner model predictions in grey: Woodhouse *et al.* (1986) as Wh; Durek & Romanowicz (1999) as DR; Tromp (1993) as Tr; and Beghein & Trampert (2003) as BT.

mode branch (Fig. 8f). It is interesting to note that placing finite Q_κ in the lithosphere, will only produce significant changes if the Q_κ values are around or below 100, and will mainly affect $_0S_0$. All of the synthetic Q_κ profiles have a poor fit with mode $_2S_0$, possibly because of its strong cross-coupling with mode $_7S_2$. Even though finite Q_κ in either the lower mantle or the outer core alone can explain the radial modes observations, both Rayleigh waves and PKP-type modes, which also have significant sensitivity to bulk attenuation, prefer finite Q_κ to be placed in the upper mantle (Durek & Ekström 1995). Based on this, we propose that our best possible synthetic scenario is setting Q_κ=1300 in the upper mantle and lithosphere (Fig. 8g), following the depth parametrization of the 1-D Q model QL6 (Durek & Ekström 1996). The selected 1-D Q_μ profile also has an effect in the Q value predictions of radial modes, however, it is beyond the scope of this paper to find the best-fitting 1-D Q_μ model for the radial modes and other types of data.

We also compare our radial mode observations to previous 1-D Q_κ and Q_μ models based on normal modes (Widmer *et al.* 1991; Durek & Ekström 1995, 1996; Resovsky *et al.* 2005). We exclude the most recent model by de Wit *et al.* (2014), as it did not include any radial mode measurements in its construction. Previous models agree rather well on the 1-D Q_μ profile, but vary significantly for Q_κ, ranging in location and several orders in magnitude for the finite Q_κ (Fig. 7). All models underpredict the Q value of $_0S_0$ (Fig. 8h), even when compared to previous observations used to build model QM1 (Widmer *et al.* 1991). In particular, RTH, the most likely model of Resovsky *et al.*'s (2005) probabilistic study, predicts a Q value for mode $_0S_0$ of just 3700, much lower than any measurement of $_0S_0$. Our observation of mode $_0S_0$ indicates that less bulk attenuation (higher Q_κ) is needed to explain the radial mode Q value observations. This matches our synthetic tests, where our proposed best scenario has Q_κ = 1300 in the upper mantle and lithosphere, much higher than Q_κ = 943 in model QL6.

The fact that mode $_0S_0$ is completely dominated by bulk attenuation, makes it a particularly interesting and important mode to analyse. We used 25 stations (Table 3), containing 2000 hr of uninterrupted data, and measured a Q value of 5982^{+211}_{-174}, which is higher than other recent measurements (Widmer *et al.* 1991; Laske *et al.* 2005; Okal & Stein 2009). However, our measurement is, within error bars, as large as older measurements of Riedesel *et al.* (1980) with 5700 ± 285, and Zürn *et al.* (1980) and Knopoff *et al.* (1979)

with 6687 ± 869. Given the mode's importance when modelling Q_κ, we confirmed our Q value observation of ${}_0S_0$ by re-measuring it in the time domain using 23 out of our 25 available stations following the method of Okal & Stein (2009), who only included data from the great 2004 Sumatra earthquake. We obtain a value of $Q = 6018^{+72}_{-42}$ by measuring the modes' decay rate in the time domain, which agrees with our measured value in the frequency domain. Special attention should be given to mode ${}_0S_0$ when modelling 1-D Q_κ and calculating its uncertainties, as this mode is particularly sensitive to Q_κ strength and location in the Earth.

5.2 Radial anisotropy in the inner core

Centre frequencies of radial modes have previously been used to constrain inner core radial anisotropy (Lythgoe & Deuss 2015). Radial anisotropy results in seismic waves travelling at different velocities along the direction of the Earth's radius and perpendicular to it. This type of anisotropy might be present in the upper most 100 km of the inner core and caused by the alignment of crystals at the surface of the inner core, due to deformation induced by flow stresses and resulting in a fast velocity axis along the Earth's radius (Yoshida *et al.* 1996).

In Fig. 9, we compare our SC and GC results to the f_c predictions generated by Lythgoe & Deuss (2015). In their calculations, they vary radial anisotropy in the upper most 100 km of the inner core by changing the parameter $\phi = v^2_{pv}/v^2_{ph}$, which changes the proportion between the velocity of compressional waves travelling vertically (v_{pv}) and horizontally (v_{ph}) with respect to the inner core boundary (ICB). Both our SC and GC results agree with a fast axis along the Earth's radius. However, our results in GC are consistent with lower values of radial anisotropy than previously found by Lythgoe & Deuss (2015). For example, ${}_5S_0$ now only requires around 4 per cent radial anisotropy instead of 9 per cent. Thus, radial mode centre frequencies measured in SC will result in an overestimation of its radial anisotropy. It is important to note, however, that the isotropic mantle model S20RTS predicts opposite values for the f_c shifts than the observations and radial anisotropy predictions. This difference indicates that the radial mode centre frequency observations are more likely due do radial inner core anisotropy than isotropic mantle structure. Moreover, if we take isotropic mantle structure into account even larger values of radial anisotropy would be required to fit our observations.

5.3 Inner core cylindrical anisotropy

In addition to radial inner core anisotropy, we can also relate our results to cylindrical inner core anisotropy. Previous studies of the Earth's inner core have shown cylindrical velocity anisotropy, with the fast axis roughly aligned to the axis of rotation. In normal modes, this is evidenced by a strong zonal degree-two and degree-four structure, which means positive variations in the polar regions, and negative ones in the equatorial area. Here, we explore this effect through our observations of cross-coupled splitting functions for radial modes and inner core sensitive $l = 2$ modes (pairs ${}_nS_0$-${}_mS_2$), as they couple both through ellipticity and degree-two structure inner core anisotropy. These cross-coupled mode pairs exhibit the same cylindrical anisotropy behaviour as inner core sensitive modes. Most remarkably, by measuring the cross-coupling between the radial and $l = 2$ modes, we observe inner core structure, which is consistent with previous inner core anisotropy models. This is specially the case for pairs where the $l = 2$ mode is mostly sensitive to inner core compressional velocity v_p, such as ${}_5S_0$-${}_{13}S_2$ and ${}_{11}S_0$-${}_{27}S_2$ (Fig. 5c). On the other hand, $l = 2$ modes, which are mostly sensitive to shear velocity v_s, are often largely overpredicted by current inner core anisotropy models (see modes ${}_7S_2$, ${}_{10}S_2$, ${}_{11}S_2$ and their cross-coupling in Figs 10a–c). This comes as a result of current inner core models being mainly based on v_p modes sensitive to the shallow inner core, which makes them unable to provide robust predictions for v_s sensitive modes. From the available inner core models, we find that all are consistent with all our cross-coupling measurements, with the exception of modes ${}_{10}S_2$ and ${}_{11}S_2$ and their cross-coupling that are not well constrained by any of the models (Fig. 10). Thus, important constraints on inner core cylindrical anisotropy can also be obtained from cross-coupling inner core sensitive modes with radial modes, such as mode pairs ${}_2S_0$-${}_7S_2$, ${}_5S_0$-${}_{13}S_2$ and ${}_{11}S_0$-${}_{27}S_2$ (Figs 5c and 6).

6 CONCLUSIONS

Unlike previous studies, we measure radial modes not only in SC, but also cross-coupled to their closest $l = 2$ spheroidal modes for degree-two structure. We include multiple earthquakes in our measurements, whereas studies before were only able to include either one or two events. By introducing more earthquake data into our measurements, we improve our knowledge of bulk attenuation Q_κ, as we remove potential earthquake bias from our results. Mode ${}_0S_0$, which is dominated by Q_κ, has a measured Q value of 5982, which is higher than in previous measurements. This indicates that less bulk attenuation, than previously thought, is required in the Earth to explain the observed Q values of radial modes. Other radial modes are not as sensitive to changes in 1-D Q_κ, but are also consistent with less bulk attenuation.

Including cross-coupling in our radial mode measurements results in a systematic shift of the centre frequencies of the radial modes closer to those of PREM. These f_c changes, that result from the cross-coupling of modes, have implications on the strength of the radial anisotropy present in the upper most inner core. Our results in GC agree with lower values of radial anisotropy than the ones inferred from just SC. In addition, cross-coupling between radial modes and $l = 2$ inner core sensitive modes provide constraints on cylindrical anisotropy, that will help us improve our knowledge of the 3-D structure of the inner core.

ACKNOWLEDGEMENTS

This project has received funding from the European Research Council (ERC) under the European Union's Horizon 2020 research and innovation programme (grant agreement no. 681535—ATUNE) and a Vici award number 016.160.310/526 from the Netherlands organisation for scientific research (NWO). The facilities of IRIS Data Services, and specifically the IRIS Data Management Centre, were used for access to waveforms, related metadata and/or derived products used in this study. IRIS Data Services are funded through the Seismological Facilities for the Advancement of Geoscience (SAGE) Award of the National Science Foundation under cooperative support agreement EAR-1851048. We also acknowledge the 'Global CMT project' webpage for the earthquake source parameters used in this study (Dziewonski *et al.* 1981, 2012). The data analysis and figures were generated using Obspy (Beyreuther *et al.* 2010) and a Python package designed by Simon Schneider, Lisanne Jagt and STS.

REFERENCES

Anderson, D. & Hart, R., 1978. Q of the Earth, *J. Geophys. Res.: Solid Earth,* **83**(B12), 5869–5882.

Andrews, J., Deuss, A. & Woodhouse, J., 2006. Coupled normal-mode sensitivity to inner-core shear velocity and attenuation, *J. Geophys. Int.,* **167**(1), 204–212.

Beghein, C. & Trampert, J., 2003. Robust normal mode constraints on inner-core anisotropy from model space search, *Science,* **299**(5606), 552–555.

Beyreuther, M., Barsch, R., Krischer, L., Megies, T., Behr, Y. & Wassermann, J., 2010. Obspy: A Python toolbox for seismology, *Seismol. Res. Lett.,* **81**(3), 530–533.

Buland, R., Berger, J. & Gilbert, F., 1979. Observations from the ida network of attenuation and splitting during a recent earthquake, *Nature,* **277,** 358–362.

Dahlen, F., 1968. The normal modes of a rotating, elliptical Earth, *J. Geophys. Int.,* **16**(4), 329–367.

Dahlen, F., 1982. The effect of data windows on the estimation of free oscillation parameters, *J. Geophys. Int.,* **69**(2), 537–549.

de Wit, R., Käufl, P., Valentine, A. & Trampert, J., 2014. Bayesian inversion of free oscillations for Earth's radial (an)elastic structure, *Phys. Earth Planet. Inter.,* **237,** 1–17.

Deuss, A. & Woodhouse, J.H., 2001. Theoretical free-oscillation spectra: the importance of wide band coupling, *J. Geophys. Int.,* **146**(3), 833–842.

Deuss, A., Irving, J.C. & Woodhouse, J.H., 2010. Regional variation of inner core anisotropy from seismic normal mode observations, *Science,* **328**(5981), 1018–1020.

Deuss, A., Ritsema, J. & van Heijst, H., 2013. A new catalogue of normal-mode splitting function measurements up to 10 mHz, *J. Geophys. Int.,* **193**(2), 920–937.

Dratler, J., Farrell, W., Block, B. & Gilbert, F., 1971. High-Q overtone modes of the Earth, *J. Geophys. Int.,* **23**(4), 399–410.

Durek, J.J. & Ekström, G., 1995. Evidence of bulk attenuation in the asthenosphere from recordings of the Bolivia Earthquake, *Geophys. Res. Lett.,* **22**(16), 2309–2312.

Durek, J.J. & Ekström, G., 1996. A radial model of anelasticity consistent with long-period surface-wave attenuation, *Bull. Seism. Soc. Am.,* **86**(1A), 144–158.

Durek, J.J. & Romanowicz, B., 1999. Inner core anisotropy inferred by direct inversion of normal mode spectra, *J. geophys. Int.,* **139**(3), 599–622.

Dziewonski, A. & Anderson, D., 1981. Preliminary Reference Earth Model, *Phys. Earth Planet. Inter.,* **25**(4), 297–356.

Dziewonski, A. & Gilbert, F., 1972. Observations of normal modes from 84 recordings of the Alaskan Earthquake of 1964 March 28, *Geophys. J. R. Astr. Soc.,* **27**(4), 393–446.

Dziewonski, A. & Gilbert, F., 1973. Observations of normal modes from 84 recordings of the Alaskan Earthquake of 1964 March 28th. Further remarks based on new spheroidal overtone data, *J. Geophys. Int.,* **35**(4), 401–437.

Dziewonski, A.M., Chou, T.-A. & Woodhouse, J.H., 1981. Determination of earthquake source parameters from waveform data for studies of global and regional seismicity, *J. Geophys. Res.: Solid Earth,* **86**(B4), 2825–2852.

Dziewonski, A.M., Ekström, G. & Nettles, M., 2012. The global CMT project 2004-2010: centroid-moment tensors for 13,017 earthquakes, *Phys. Earth Planet. Inter.,* **200,** 1–9.

Edmonds, A.R., 1960. *Angular Momentum in Quantum Mechanics,* Princeton Univ. Press.

Giardini, D., Li, X.-D. & Woodhouse, J.H., 1988. Splitting functions of long-period normal modes of the Earth, *J. Geophys. Res.: Solid Earth,* **93**(B11), 13716–13742.

Gilbert, F. & Dziewonski, A.M., 1975. An application of normal mode theory to the retrieval of structural parameters and source mechanisms from seismic spectra, *Philos. Trans. R. Soc. Lond. Ser. A, Math. Phys. Sci.,* **278**(1280), 187–269.

He, X. & Tromp, J., 1996. Normal-mode constraints on the structure of the Earth, *J. Geophys. Res.: Solid Earth,* **101**(B9), 20053–20082.

Irving, J., Deuss, A. & Andrews, J., 2008. Wide-band coupling of Earth's normal modes due to anisotropic inner core structure, *J. Geophys. Int.,* **174**(3), 919–929.

Knopoff, L., Rydelek , P.A., Zürn , W. & Yogi, T., 1979. Q of mode $_0S_0$, *J. Geophys.—IF 32.18,* **46**(1), 89–95.

Koelemeijer, P., Deuss, A. & Ritsema, J., 2013. Observations of core-mantle boundary Stoneley modes, *Geophys. Res. Lett.,* **40**(11), 2557–2561.

Koelemeijer, P., Ritsema, J., Deuss, A. & Van Heijst, H.-J., 2016. SP12RTS: a degree-12 model of shear-and compressional-wave velocity for Earth's mantle, *J. Geophys. Int.,* **204**(2), 1024–1039.

Laske, G., Masters, G. & Dziewonski, A., 2001. New measurements of radial mode eigenfrequencies, in AGU Fall Meeting Abstracts, S32B–-0629.

Laske, G., Dziewonski, A. & Masters, G., 2005. The Reference Earth Model website. Available at: http://mahi.ucsd.edu/Gabi/rem.html, (access December 2018).

Lythgoe, K.H. & Deuss, A., 2015. The existence of radial anisotropy in Earth's upper inner core revealed from seismic normal mode observations, *Geophys. Res. Lett.,* **42**(12), 4841–4848.

Majstorović, J., Rosat, S., Lambotte, S. & Rogister, Y., 2019. Testing performances of the optimal sequence estimation and autoregressive method in the frequency domain for estimating eigenfrequencies and zonal structure coefficients of low-frequency normal modes, *J. Geophys. Int.,* **216**(2), 1157–1176.

Mäkinen, A.M. & Deuss, A., 2013. Normal mode splitting function measurements of anelasticity and attenuation in the Earth's inner core, *J. Geophys. Int.,* **194**(1), 401–416.

Masters, G. & Gilbert, F., 1983. Attenuation in the Earth at low frequencies, *Philos. Trans. R. Soc. Lond. Ser. A, Math. Phys. Sci.,* **308**(1504), 479–522.

Masters, T. & Widmer, R., 1995. Free oscillations: frequencies and attenuations, in *Global Earth Physics: A Handbook of Physical Constants,* Vol. **1,** p. 104. American Geophysical Union., ed. T.J., Ahrens.

Mooney, W., Laske, G. & Masters, G., 1998. CRUST5.1: a global model at 5 degrees by 5 degrees, *J. Geophys. Res,* **102,** 727–748.

Moulik, P. & Ekström, G., 2014. An anisotropic shear velocity model of the Earth's mantle using normal modes, body waves, surface waves and long-period waveforms, *J. Geophys. Int.,* **199**(3), 1713–1738.

Okal, E.A., 1996. Radial modes from the great 1994 bolivian earthquake: no evidence for an isotropic component to the source, *Geophys. Res. Lett.,* **23**(5), 431–434.

Okal, E.A. & Stein, S., 2009. Observations of ultra-long period normal modes from the 2004 Sumatra–Andaman Earthquake, *Phys. Earth planet. Inter.,* **175**(1), 53–62.

Pachhai, S., Masters, G. & Laske, G., 2020. Probabilistic estimation of structure coefficients and their uncertainties, for inner-core sensitive modes, using matrix autoregression, *J. Geophys. Int.,* **221,** 1366–1383

Park, J., 1990. Radial mode observations from the 5/23/89 Macquarie Ridge Earthquake, *Geophys. Res. Lett.,* **17**(7), 1005–1008.

Resovsky, J. & Ritzwoller, M., 1998. New and refined constraints on three-dimensional Earth structure from normal modes below 3 mHz, *J. Geophys. Res.: Solid Earth,* **103**(B1), 783–810.

Resovsky, J., Trampert, J. & Van der Hilst, R., 2005. Error bars for the global seismic Q profile, *Earth Planet. Sci. Lett.,* **230**(3), 413–423.

Riedesel, M.A., Agnew, D., Berger, J. & Gilbert, F., 1980. Stacking for the frequencies and Qs of $_0S_0$ and $_1S_0$, *J. Geophys. Int.,* **62**(2), 457–471.

Ritsema, J., van Heijst, H.J. & Woodhouse, J.H., 1999. Complex shear wave velocity structure imaged beneath Africa and Iceland, *Science,* **286**(5446), 1925–1928.

Ritsema, J., Deuss, A., Van Heijst, H. & Woodhouse, J., 2011. S40RTS: a degree-40 shear-velocity model for the mantle from new Rayleigh wave dispersion, teleseismic traveltime and normal-mode splitting function measurements, *J. Geophys. Int.,* **184**(3), 1223–1236.

Romanowicz, B. & Durek, J.J., 2000. Seismological constraints on attenuation in the Earth: a review, *Earth's Deep Interior: Mineral Physics and Tomography from the Atomic to the Global Scale,* **117,** pp. 161–179, American Geophysical Union, Karato , Shun-Ichiro, Forte , Alessandro, Liebermann , Robert , Masters, Guy & Stixrude, Lars.

Rosat, S., Watada, S. & Sato, T., 2007. Geographical variations of the ${}_0S_0$ normal mode amplitude: predictions and observations after the Sumatra-Andaman earthquake, *Earth Planets Space,* **59**(4), 307–311.

Roult, G., Roch, J. & Clévédé, E., 2010. Observation of split modes from the 26th December 2004 Sumatra–Andaman mega-event, *Phys. Earth Planet. Inter.,* **179**(1), 45–59.

Sailor, R.V. & Dziewonski, A.M., 1978. Measurements and interpretation of normal mode attenuation, *J. Geophys. Int.,* **53**(3), 559–581.

Talavera-Soza, S. & Deuss, A., 2020. Constraining 1-D inner core attenuation through measurements of strongly coupled normal mode pairs, *J. Geophys. Int.,* **223**(1), 612–621.

Tarantola, A. & Valette, B., 1982. Generalized nonlinear inverse problems solved using the least squares criterion, *Rev. Geophys.,* **20**(2), 219–232.

Tromp, J., 1993. Support for anisotropy of the Earth's inner core from free oscillations, *Nature,* **366**(6456), 678–681.

Widmer, R., Masters, G. & Gilbert, F., 1991. Spherically symmetric attenuation within the Earth from normal mode data, *J. Geophys. Int.,* **104**(3), 541–553.

Woodhouse, J., 1980. The coupling and attenuation of nearly resonant multiplets in the Earth's free oscillation spectrum, *J. Geophys. Int.,* **61**(2), 261–283.

Woodhouse, J., 1988. The calculation of the eigenfrequencies and eigenfunctions of the free oscillations of the Earth and Sun, in *Seismological Algorithms: Computational Methods and Computer Programs,* pp. 321–370, Doornbos , Durk, Academic Press.

Woodhouse, J. & Dahlen, F., 1978. The effect of a general aspherical perturbation on the free oscillations of the Earth, *J. Geophys. Int.,* **53**(2), 335–354.

Woodhouse, J. & Giardini, D., 1985. Inversion for the splitting function of isolated low order normal mode multiplets, *EOS Trans. Am. geophys. Un.,* **66,** 300.

Woodhouse, J., Giardini, D. & Li, X.-D., 1986. Evidence for inner core anisotropy from free oscillations, *Geophys. Res. Lett.,* **13**(13), 1549–1552.

Yoshida, S., Sumita, I. & Kumazawa, M., 1996. Growth model of the inner core coupled with the outer core dynamics and the resulting elastic anisotropy, *J. Geophys. Res.: Solid Earth,* **101**(B12), 28085–28103.

Zürn, W., Knopoff, L. & Rydelek, P. A., 1980. High precision measurement of the frequency of mode ${}_0S_0$, *J. Geophys.—IF 32.18,* **48**(1), 158–160.

SUPPORTING INFORMATION

Supplementary data are available at *GJI* online.

Figure S1 Recovery tests where we use synthetic data to measure f_c and Q in SC (red) and GC (black) plotted with respect to PREM. The synthetic data are calculated including cross-coupling for ellipticity between the radial modes and their corresponding $l = 2$ modes (Table 2) in addition to centre frequency shifts for the radial modes. The centre frequencies measured from the synthetic data using GC (red) match the input centre frequency shifts in the synthetics (grey), while all measurements made using only SC find centre frequency shifts from PREM which are too large, just like in our real data measurements. The Q values measured using the synthetic data do not show a systematic difference between SC and GC recovered values. The biggest difference between SC and GC recovered Q values is visible for ${}_2S_0$-${}_7S_2$ and ${}_{11}S_0$-${}_{27}S_2$, which are both strongly cross-coupled modes pars and are close in frequency. We are not able to fully recover the Q values of ${}_0S_0$, ${}_3S_0$ and ${}_4S_0$, even when we are using GC, which we believe is because of insufficient spectral segments. We include the GC Q value deviations from the synthetic test in our uncertainties of these modes.

Figure S2 Recovery tests using synthetic data which include cross-coupled splitting functions. The left-hand column shows the cross-coupled splitting functions used to calculate the synthetic spectra. The right-hand column shows the cross-coupled splitting functions measured from these synthetic spectra. Even though cross-coupled structure was included in the synthetic spectra calculation, it was not recovered in the measured splitting functions. In the test, we used the same set-up as what we use to measure cross-coupling in real data, including different frequency windows for both modes. Both in the real data and in the synthetic test shown here, we were not able to recover any cross-coupling between radial mode ${}_0S_0$ and ${}_2S_2$, ${}_1S_2$ or ${}_0S_5$.

Figure S3 Comparison between our SC splitting functions measurements of $l = 2$ modes, measured in GC with their respective radial modes, with predictions for a combined mantle and inner core anisotropy model using Tromp (1993, second column), and previous SC measurement by Deuss *et al.* (2013, third column) and Pachhai *et al.* (2020, fourth column).

Figure S4 Radial mode sensitivity kernels as a function of depth for shear attenuation q_μ in red ($\mu_0 K_\mu$) and bulk attenuation q_κ in black ($\kappa_0 K_\kappa$), calculated for PREM. The transition zone (TZ), core mantle boundary (CMB) and inner core boundary (ICB) are marked in figure.

Table S1 List of seismic networks we use in our measurements. Also listed, how many stations we select from the availability of each network.

Please note: Oxford University Press is not responsible for the content or functionality of any supporting materials supplied by the authors. Any queries (other than missing material) should be directed to the corresponding author for the paper.